International Journal of Pharmaceutics 382 (2009) 296–304

Contents lists available at ScienceDirect

International Journal of Pharmaceutics

journal homepage: www.elsevier.com/locate/ijpharm

Pharmaceutical Nanotechnology

Production of hybrid lipid-based particles loaded with inorganic nanoparticles and active compounds for prolonged topical release

C.A. García-González[a,*], A.R. Sampaio da Sousa[b], A. Argemí[c], A. López Periago[a], J. Saurina[c], C.M.M. Duarte[b,d], C. Domingo[a,*]

[a] Instituto de Ciencia de Materiales de Barcelona (CSIC), Campus de la UAB s/n, E-08193 Bellaterra, Spain
[b] Instituto de Biologia Experimental e Tecnológica (IBET), Aptd. 12, 2781-901 Oeiras, Portugal
[c] Department of Analytical Chemistry, University of Barcelona, Diagonal 647, E-08028 Barcelona, Spain
[d] Instituto de Tecnologia Química e Biológica (ITQB), Av. República (EAN), 2780-157 Oeiras, Portugal

ARTICLE INFO

Article history:
Received 17 June 2009
Received in revised form 20 August 2009
Accepted 24 August 2009
Available online 29 August 2009

Keywords:
Supercritical fluid
Solid lipid particles
Sunscreen
Caffeine
Particle design
Eutectic mixture

ABSTRACT

The production of particulate hybrid carriers containing a glyceryl monostearate (Lumulse® GMS-K), a waxy triglyceride (Cutina® HR), silanized TiO_2 and caffeine were investigated with the aim of producing sunscreens with UV-radiation protection properties. Particles were obtained using the supercritical PGSS® (Particles from Gas Saturated Solutions) technique. This method takes advantages of the lower melting temperatures of the lipids obtained from the dissolution of CO_2 in the bulk mixture. Experiments were performed at 13 MPa and 345 K, according to previous melting point measurements. Blends containing Lumulse® GMS-K and Cutina® HR lipids (50 wt%) were loaded with silanized TiO_2 and caffeine in percentile proportions of 6 and 4 wt%, respectively. The particles produced were characterized using several analytical techniques as follows: system crystallinity was checked by X-ray diffraction and differential scanning calorimetry, thermal stability by thermogravimetric analysis, and morphology by scanning and transmission electron microscopy. Further, the UV-shielding ability of TiO_2 after its dispersion in the lipidic matrix was assessed by solid UV–vis spectroscopy. Preliminary results indicated that caffeine-loaded solid lipid particles presented a two-step dissolution profile, with an initial burst of 60 wt% of the loaded active agent. Lipid blends loaded with TiO_2 and caffeine encompassed the UV-filter behavior of TiO_2 and the photoaging prevention properties of caffeine.

1. Introduction

The use of complex lipids composed by different molecules is currently a common choice in terms of preparation of novel controlled release systems with excellent pharmacological and therapeutic properties (Savolainen et al., 2002; Davis, 2004; Ljusberg-Wahren et al., 2005). For both pharmaceutical and cosmetic applications, solid lipid particles have advantages over other carriers, such as liposomes or emulsions, in terms of stability and protection of the incorporated active compounds (Müller et al., 2000). The research activity on solid lipid particles has gradually focused on cosmetic and topical products (Müller et al., 2002; Puglia et al., 2008; Pardeike et al., 2009). At the same time, the development of dermal formulations for protection from UV-radiation, incorporating organic UV-absorbers and inorganic UV-blockers, has become a topic of increasing concern in human life. Among the used inorganic UV-blockers, nanoparticulate titanium dioxide (TiO_2) is widely employed in creams containing lipids, because of the broad UV-spectrum coverage of TiO_2 (Lowe et al., 1997; Hexsel et al., 2008), and because solid lipids can also act as UV sunscreen systems (Yener et al., 2003; Villalobos-Hernández and Müller-Goymann, 2005; Pardeike et al., 2009). However, one of the major challenges for preparing homogeneous creams involving dispersed inorganic phases is to avoid the segregation of the mineral component from the oil phase (Chen et al., 2006; Pardeike et al., 2009). Further, life cycle impact assessment studies of nanometric materials intended for dermal use give advice of encapsulating the nanoparticles into larger particles to minimize the potential negative environmental and health impacts (Klöpffer, 2007; Grobe et al., 2008). In this context, the use of solid lipid microparticles entrapping TiO_2 nanoparticles could accomplish both tasks: to reduce the risk of nanoparticles toxicity and to help dispersing the nanoparticles into the organic phase; while, simultaneously, contribute to optimize the UV-filter ability of the mixture. Hence, this work is primarily focused on the preparation of a composite comprising solid lipid particles and dispersed TiO_2 with applications in sunscreens free of organic absorbers. Moreover, solid lipid parti-

* Corresponding authors. Tel.: +34 93 5801853; fax: +34 93 5805729.
E-mail addresses: cgarcia@icmab.es (C.A. García-González), conchi@icmab.es (C. Domingo).

0378-5173/$ – see front matter © 2009 Elsevier B.V. All rights reserved.
doi:10.1016/j.ijpharm.2009.08.033

cles have a great potential as vehicles for topical administration of active substances, principally owing to the possible targeting effect and controlled release in different skin strata (Müller et al., 2000, 2002). In the present study, advantageous solid lipid particles features for topical administration of caffeine were also considered in a preliminary study. Caffeine was selected as a model hydrophilic active drug because of its protective effects against UV-B radiation (Staniforth et al., 2006), anticellulite activity (Bertin et al., 2001) and photoaging prevention capacity (González et al., 2008), all useful features in dermal applications. The long-term aim of our work is to explore novel lipid formulations with skin targeting effect for the treatment of skin diseases (e.g., delivery of caffeine for the treatment of psoriasis (Vali et al., 2005)) or skin cancer prevention (Staniforth et al., 2006) that might benefit from topical administration, obtaining a substantial reduction of the systemic side effects.

For pharmaceutical and cosmetic products, there is an increased interest in developing technologies that allow the production of particles with controlled particle-size distribution and product quality (crystallinity, purity, morphology, etc.) under mild and clean conditions. Current methods of making solid lipid particles for pharmaceutical applications include fusion processes, cold or hot high-pressure homogenization and multi-step solvent processes, such as emulsification and ultrasonication (Gasco, 1997; Müller et al., 2000; Sethia and Squillante, 2004; Chattopadhyay et al., 2007). Technologies based on supercritical carbon dioxide ($scCO_2$), and in particular the PGSS® (Particles from Gas Saturated Solutions) (Weidner et al., 1995) process, have emerged as alternative one-step methods to obtain solvent-free solid lipid particles at low processing temperatures (Weidner et al., 1995; Rodrigues et al., 2004; Calderone et al., 2007; Sampaio de Sousa et al., 2007, 2009; Temelli, 2009). In this study, the PGSS® process was first used to disperse TiO_2 nanoparticles into solid lipid microparticles. The technique consisted in dissolving $scCO_2$ in the bulk of a melted lipid mixture with dispersed TiO_2 nanoparticles, and the subsequent quick expansion through a nozzle, causing the complete evaporation of the gas and the solidification of the liquid suspension. A silane adhesion promoter was previously deposited as a primer on the hydrophilic surface of TiO_2 to enhance its dispersion capacity (Plueddemann, 1991). The lipids selected for study were Lumulse® GMS-K and Cutina® HR. Lumulse® GMS-K is a glyceryl monostearate with a C_{18} alkyl chain. It is used in cosmetics and pharmaceutical dermal products as a lipophilic surfactant, emulsifier and humectant agent (Gopala Krishna, 1993). Cutina® HR (hydrogenated castor oil) is a highly hydrophobic waxy triglyceride sterified with three C_{18} fatty acids, which is often used as a drug carrier for topical applications (Ogunniyi, 2006; Jannin et al., 2008). Progressing on the complexity of the designed system, solid lipid particles loaded with caffeine and silanized TiO_2 were also processed using the PGSS® technique.

2. Materials and methods

2.1. Materials

Lumulse® GMS-K (GMS) and Cutina® HR (HCO) were kindly provided by Lambent Technologies and José M. Vaz Pereira S.A., respectively. TiO_2 nanometric particles (~20 nm in diameter) were supplied by Degussa (TiO_2 P25). Octyltriethoxysilane (TiC_8) and octadecyltrimethoxysilane (TiC_{18}) coated TiO_2 nanoparticles were prepared in our laboratory following a $scCO_2$ reported procedure (García-González et al., 2009a,b). Caffeine (Caff, >98 wt% purity) was purchased from Sigma Aldrich. CO_2 (99.998 mol% purity) was supplied by Air Liquide.

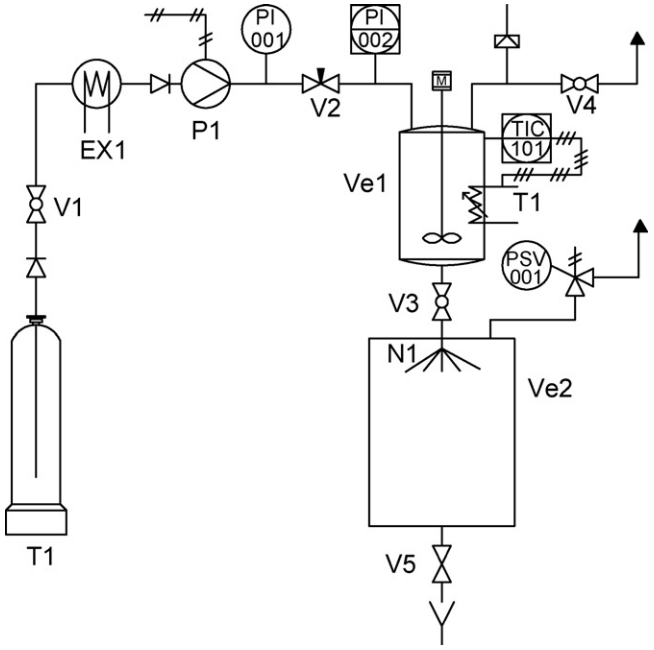

Fig. 1. Process flow diagram of the equipment used for PGSS® lipid particle formation. T1: CO_2 reservoir, EX1: CO_2 cooling unit, P1: pump, V1–V5: valves, Ve1: high-pressure mixing chamber, Ve2: collector vessel, T1: heater, N1: nozzle.

2.2. Experimental procedure

Unloaded and loaded (caffeine and/or TiO_2) solid lipid particles were produced using the high-pressure equipment depicted in Fig. 1. CO_2 was fed by a high-pressure piston pump (P1, Haskel model MCPV-71) to a 0.5 L high-pressure stirred vessel (Ve1, Parr Instruments) containing the substances to be processed until the desired working pressure was reached (13 MPa). The autoclave was heated at 345 K by a thin band heater (T1, Watlow STB3J2J1). After 1 h of stirring, necessary for mixture equilibration, the system was depressurized by opening valve V3 (Parker 4M4Z-B2LJ) and atomized through a 600 μm cone nozzle (N1, Spraying Systems Co.) into a 10 L atmospheric collector (Ve2) where particles were recovered.

2.3. Characterization

2.3.1. Lipids melting point determination

The extent of the melting point depression of the studied lipids due to CO_2 dissolution was essential information necessary to settle the operating conditions in the PGSS® process (Hammam and Sivik, 1993; Kazarian, 2000). For GMS, data of CO_2 solubility in the lipid and its influence in the melting point can be found in the literature (Sampaio de Sousa et al., 2007). On the other hand, the influence of CO_2 in the melting point of HCO was experimentally evaluated using a visual method (Fukné-Kokot et al., 2000; Sampaio de Sousa et al., 2006), since only data of CO_2 solubility in HCO were found reported (Münüklü et al., 2006). Further, the melting points of two different HCO:GMS mixtures with mass ratios of 1:1 and 3:1 were also measured using a similar method. Data were obtained using a high-pressure view cell with sapphire windows (~4 mL, Parr Instruments), in which a capillary tube containing the lipid was inserted. Liquefied CO_2 was pumped using a piston pump (Haskel 29723-71) into the cell until the desired pressure was reached. Next, the temperature was gradually increased until the complete melting of the solid compounds was visually observed. Measurements were taken up to 17 MPa for pure HCO and mixtures of GMS and HCO (HCO:GMS = 1:1 and 3:1 mass ratio).

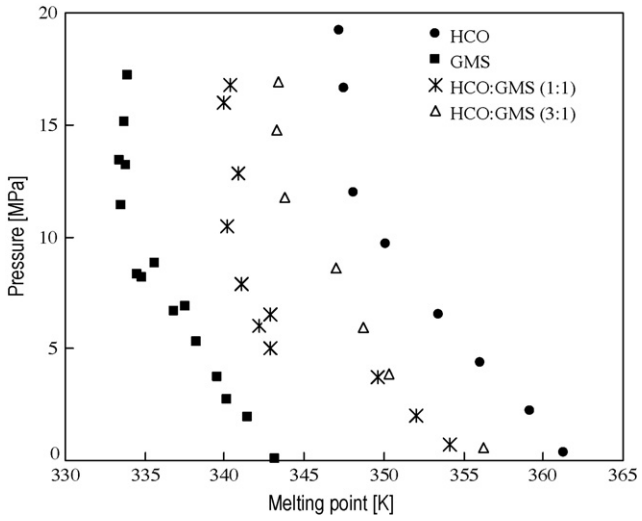

Fig. 2. Melting points of GMS (data from Sampaio de Sousa et al., 2007), HCO and HCO:GMS mixtures with mass ratios of 1:1 and 3:1 in the presence of compressed CO_2.

2.3.2. Solid lipid particles analysis

Thermal stability of obtained samples was estimated using thermogravimetric analysis (TGA, PerkinElmer 7) under Ar atmosphere raising the temperature at a rate of 5 K min^{-1}. Samples melting temperatures were measured on a differential scanning calorimeter (DSC, 822e/400 Mettler Toledo) operating at a heating rate of 10 K min^{-1} under N_2 purge. Crystallinity of obtained samples was analyzed by X-ray diffraction (XRD, Rigaku Rotaflex RU200 B instrument). A PerkinElmer Lambda 19 UV/VIS/NIR spectrophotometer, operating in the diffuse reflectance mode, was used for recording UV–vis spectra of solid samples using $BaSO_4$ as a reference. Micrographs of the samples were taken using both scanning (SEM, JEOL JSM 6300) and transmission (TEM, JEOL JEM-1210) electron microscopes. The SEM microscope was equipped with a LINK-ISIS-200 energy dispersive spectrometer (EDS, Oxford Instruments).

2.3.3. Caffeine release profile

Caffeine content within the solid lipid particles was determined by HPLC using an Agilent 1100 system furnished with a C_{18} column (Synergy Hydro-RP, Phenomenex, 150 mm × 4.6 mm i.d., particle-size 4 μm) according to a method described in literature (Sampaio de Sousa et al., 2007). Three portions of the caffeine-loaded sample were used for analysis. Caffeine was first extracted from the lipidic matrix using a water:methanol mixture (1:1 in a volume ratio). The analyte was detected spectrophotometrically at λ = 272 nm. Next, the release profile of the caffeine-loaded solid dispersion to ultrapure water (Millipore, Milford, MA, USA) was performed during 24 h and in triplicate. An accurately weighed amount (20 mg) of the solid lipid particles was placed in a vessel containing 200 mL of distilled water at 310 ± 1 K stirred at 70 rpm. Aliquots of the sample, withdrawn at different periods of time, were filtered through 0.45 μm pore size and analyzed by HPLC.

3. Results and discussion

In this work, we have first evaluated the optimal operating conditions to produce solid lipid particles of HCO and GMS and their mixtures using the PGSS® method by studying their melting point variations in the presence of CO_2 (Fig. 2). For all the studied systems, the melting point first decreased as the pressure increased due to the incorporation of gas into the bulk of the substances (Spilimbergo et al., 2006; Calderone et al., 2007; Sampaio de Sousa et al., 2007). After a certain pressure value (~12–16 MPa), the melting point was either not modified or increased slightly with increasing pressure due to the competing hydrostatic pressure effect. The optimal operating conditions for particles formation using the PGSS® process were chosen at 13 MPa and 345 K. Under these experimental conditions, blends with a percentile weight ratio HCO:GMS 75:25 wt% or lower were completely melted (Fig. 2). Finally, a mixture of HCO:GMS with a ratio 50:50 wt% was chosen for PGSS® precipitation, since raising the HCO wax weight percentage increased the melting point of the mixture and, thus, the occurrence of nozzle blockage during experiments.

A second part of the study consisted in producing solid lipid particles of binary mixtures of HCO and GMS by PGSS®, both alone and loaded with either silanized TiO_2 or silanized TiO_2 plus caffeine. In the PGSS® technique, the quick expansion of the mixture through a nozzle caused the complete separation of the CO_2 from the lipids along with the solidification of the melt due to Joule–Thomson effect (Chacín et al., 1999; Calderone et al., 2007). Fast pressure and temperature drops, occurring simultaneously, led to the formation of fine free flowing particles.

3.1. Physical state, thermal stability and morphology of precipitated solid lipid particles

HCO, GMS and the 1:1 mixture were first precipitated using the PGSS® equipment (samples referred to as sc-HCO, sc-GMS and sc-HCO:GMS) to evaluate the impact of the physical state of the studied lipids on the TiO_2 and drug incorporation capacity. The rapid evaporation of CO_2 from the lipid droplets formed during expansion through the nozzle, which in turn caused rapid lipid solidification, could influence the crystalline structures of sprayed glyceryls. During rapid cooling, lipids tend to initially crystallize in the least ordered crystal subcell structure (α-form), but then transform to a more ordered subcell structure (β′- and β-forms) (Chapman, 1962; Garti and Sato, 1988). The X-ray diffraction patterns of simple raw lipids displayed three strong reflections at 2θ ~5.4°, 19.7° and 22.1°, typical of the triclinic β polymorph of substituted glyceryls (Fig. 3a) (Kodali et al., 1985; Bunjes et al., 1996; Kumar et al., 2007). In addition, the reflection appearing at 2θ = 23.2° for GMS was assigned to the orthorhombic chain packing of the β′ polymorph (Kumar et al., 2007). In the case of simple lipids precipitated using the PGSS® technique, the only polymorphic phase observed by XRD was the β polymorph for both sc-HCO and sc-GMS lipids. In principle, the cooling rate in the PGSS® process seemed to be slow enough to allow the molecules to rearrange in the most stable β conformation. However, it should be taken into account that the diffraction patterns shown in Fig. 3a were recorded after several weeks of samples preparation. During this period, solid transformation of α- to β-form was also feasible. The X-ray reflections of crystallized sc-HCO were broader and much weaker than those of the HCO precursor. On the contrary, for the sc-GMS sample the reflection due to the β′ polymorph disappeared and the low angle β-reflection increased in intensity, thus indicating a possible higher degree of crystallinity than raw GMS. The precipitated mixed lipid matrix sc-HCO:GMS displayed the reflections of the β-modification, but the intensity of the peaks decreased with respect to sc-HCO and sc-GMS, which suggested a less ordered matrix for the mixture.

Similar results to those of XRD regarding crystallinity of the blend were derived from DSC measurements (Fig. 3b). The thermograms of raw materials revealed one single endothermic transition each one with onsets at 329 and 358 K, which corresponded to the melting of the stable β-modification of GMS and HCO, respectively. The PGSS® precipitated mixture melted with two broad endothermic transitions with onsets at 325 and 345 K. The two separated thermal maxima, both at lower temperatures than the corresponding bulk materials separately, together with the fact that the DSC

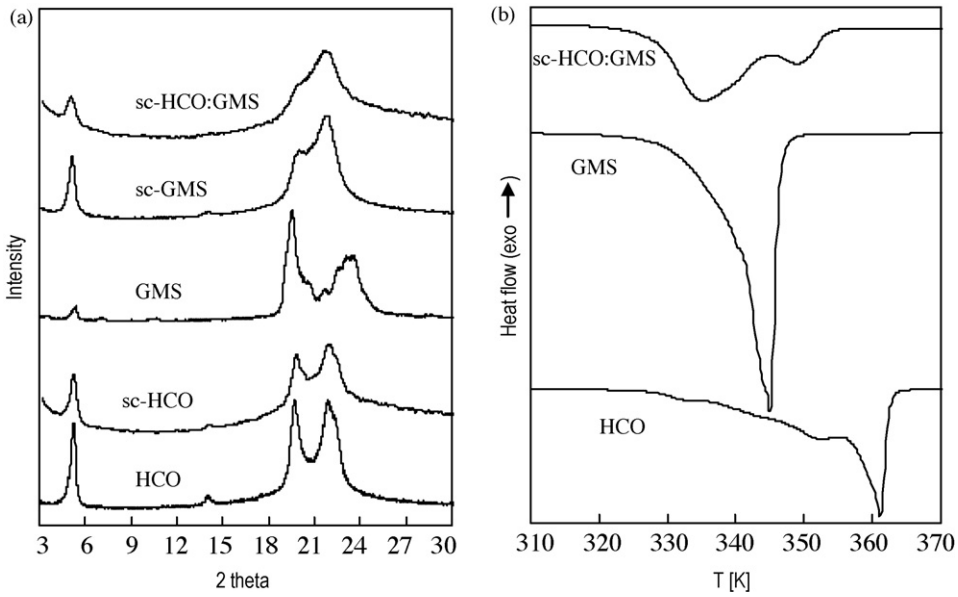

Fig. 3. Solid characterization of raw and treated lipidic materials: (a) powder XRD patterns, and (b) DSC thermograms.

thermograms did not show any exothermic cold crystallization peak corresponding to polymorphic transformation (Siekmann and Westesen, 1994; Bunjes et al., 1996), indicated the formation of an eutectic mixture rather than the creation of a miscible solid solution (Paoletti and Kritchevsky, 1967; Timms, 1984; Garti and Sato, 1988; Bunjes et al., 1996; Neubert et al., 1997; Ohta and Hatta, 2002; Himawan et al., 2006). The first transition was associated with the melting of the eutectic mixture. The onset temperature of this peak was ~325 K and can be rationalized as the dissolution of HCO in GMS, which shifted the melting temperature of the wax to lower values. The following peak arose from the melting of the excess component in the eutectic mixture, probably HCO with the highest melting temperature of the two studied lipids. Moreover, the broadening of the melting peaks in the mixture and the reduction of the melting point also indicated an increased number of lattice defects. It should be taken into account that the less perfect the lipid matrix is, the better it will be to ensure more drug loading and less drug crystallization.

Fig. 4 shows the weight loss curves obtained by thermogravimetric analysis (Fig. 4a) and the derivative of the TGA curves (Fig. 4b). Raw HCO decomposed with a single decay between 600 and 725 K. The TGA and the derivative curves corresponding to raw GMS showed three main decomposition steps between 500 and 725 K. This decomposition behavior could be related to the complex composition of Lumulse® GMS-K that contained diglycerides together with the main component glyceryl monostearate (Lumulse® GMS-K Technical Data Sheet in www.petroferm.com). The thermal stability of the processed sc-HCO slightly decreased with respect to raw HCO, since its decomposition occurred between 610 and 670 K. sc-GMS decomposed between 500 and 680 K and more gradually than raw GMS. The TGA curve of the treated sc-HCO:GMS mixture had two well resolved weight decays between 500 and 680 K, indicating similar thermal stability than sc-HCO and sc-GMS samples (Fig. 4a). The first decay started at 500 K and had the offset at 580 K with a weight loss of ~30 wt%. This weight loss was assigned to partial decomposition of the less thermally stable GMS. In this temperature interval, the weight losses of GMS and sc-GMS samples were of 30 and 20 wt%, respectively. The second decay had the maximum weight loss rate at ~670 K, a similar temperature to that of the maxima weight loss of both sc-HCO and sc-GMS.

SEM micrographs indicated that the smooth surface of raw lipids (Sampaio de Sousa et al., 2007) turned porous after PGSS® processing (Fig. 5a). For the mixture sc-HCO:GMS, porous particles of ~50–100 μm were precipitated. The microstructure observed by TEM resembled a lamellar structure (Fig. 5b), likely alternating fine layers of HCO and GMS materials in the eutectic mixture (Iwai et al., 1996). Black spots in Fig. 5b were associated with HCO precipitated separately. Lamellar structures are often observed in cases where a phase transformation front moves quickly, leaving behind two solid products, as occurred in crystallization during rapid cooling of eutectic mixtures.

3.2. Incorporation of TiO_2

The previous section described studies carried out to obtain lipid blends from rapid precipitation using the PGSS® technique. The work was herein extended to precipitate blends consisting of HCO and GMS loaded also with either bare TiO_2 or silanized nanoparticles (TiC_8 and TiC_{18}) in a mass ratio of 1:1:0.1 for the system HCO:GMS:Ti. Since the lipid blend was arranged in a lamellar lattice structure, it was expected that mineral ingredients could be stored between these layers. The maximum mass weight of TiO_2 compatible with the PGSS® process was ~5 wt%, since higher percentages led to nozzle blockage, likely due to the high viscosity of the melt containing the dispersed nanoparticles (Villalobos-Hernández and Müller-Goymann, 2005).

The weight of mineral filler (TiO_2, TiC_8 or TiC_{18}) in the composite solid lipid particles was quantified using TGA analysis after samples pyrolysis at temperatures higher than 725 K. In all of the studied samples, the percentile value of the residue at 725 K corresponded to ~6 wt% of the total composite mass (Fig. 6a). Therefore, under working experimental conditions, the sample percentile composition was maintained with respect to the initially added to the mixing chamber for PGSS® processing. TGA curves indicated that loaded blends decomposed between 500 and 680 K, a similar temperature interval to that observed for sc-HCO:GMS sample (Fig. 4b). However, slightly different thermal decomposition intervals were observed for the solid lipid particles loaded with either bare TiO_2 or silanized TiO_2. Samples filled with silanized TiO_2 had the maximum rate of thermal decomposition estimated from the derivative TGA curves at temperatures similar to that of the unfilled blend (~670

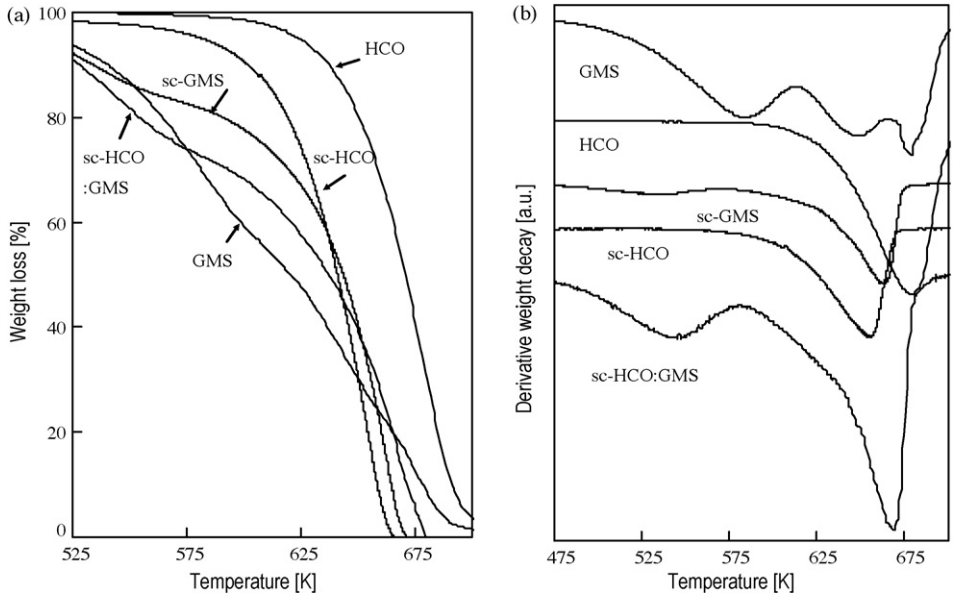

Fig. 4. Thermogravimetric curves for the decomposition of simple and mixed lipids: (a) TGA, and (b) derivative TGA curves (data are displaced on the *y*-axis for clarity reasons).

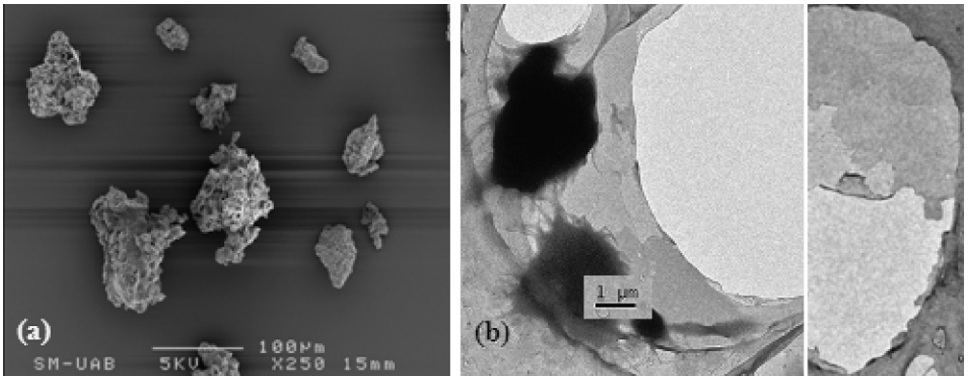

Fig. 5. Micrographs of sc-HCO:GMS precipitated particles taken by: (a) SEM, and (b) TEM.

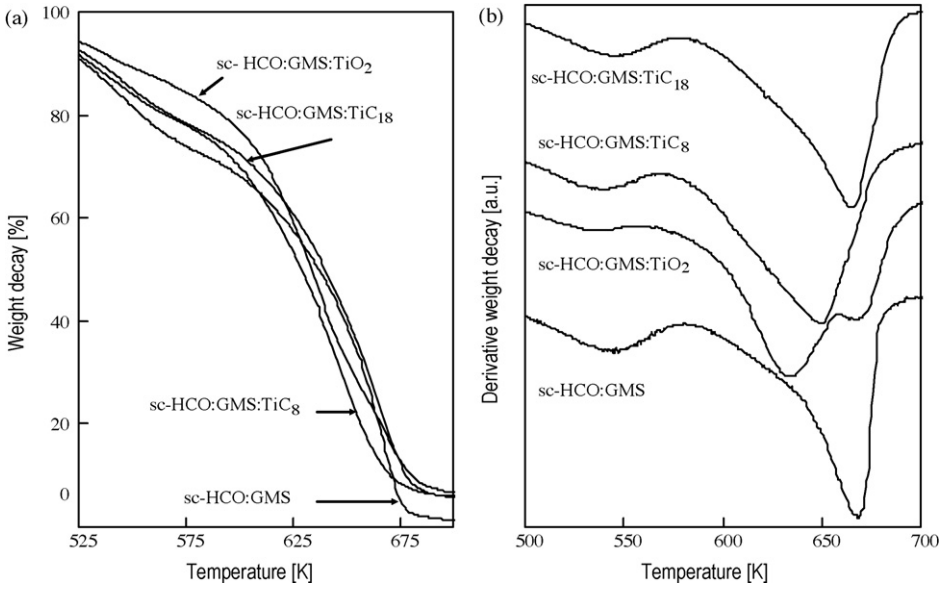

Fig. 6. Thermogravimetric curves for the decomposition of unloaded and TiO_2 loaded mixed lipids: (a) TGA, and (b) derivative TGA curves (data are displaced on the *y*-axis for clarity reasons).

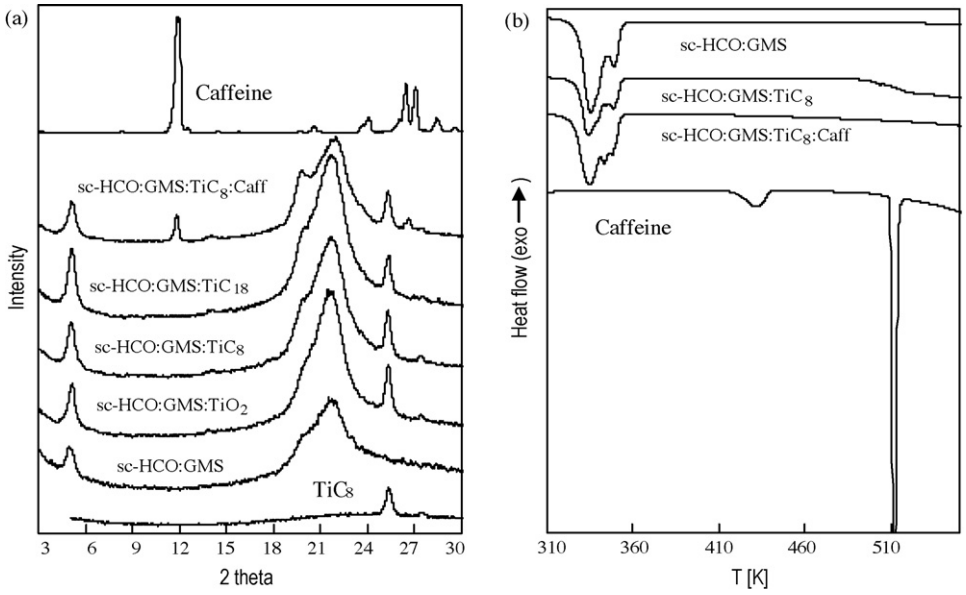

Fig. 7. Characterization of TiO_2 and caffeine-loaded lipidic materials: (a) powder XRD patterns, and (b) DSC thermograms.

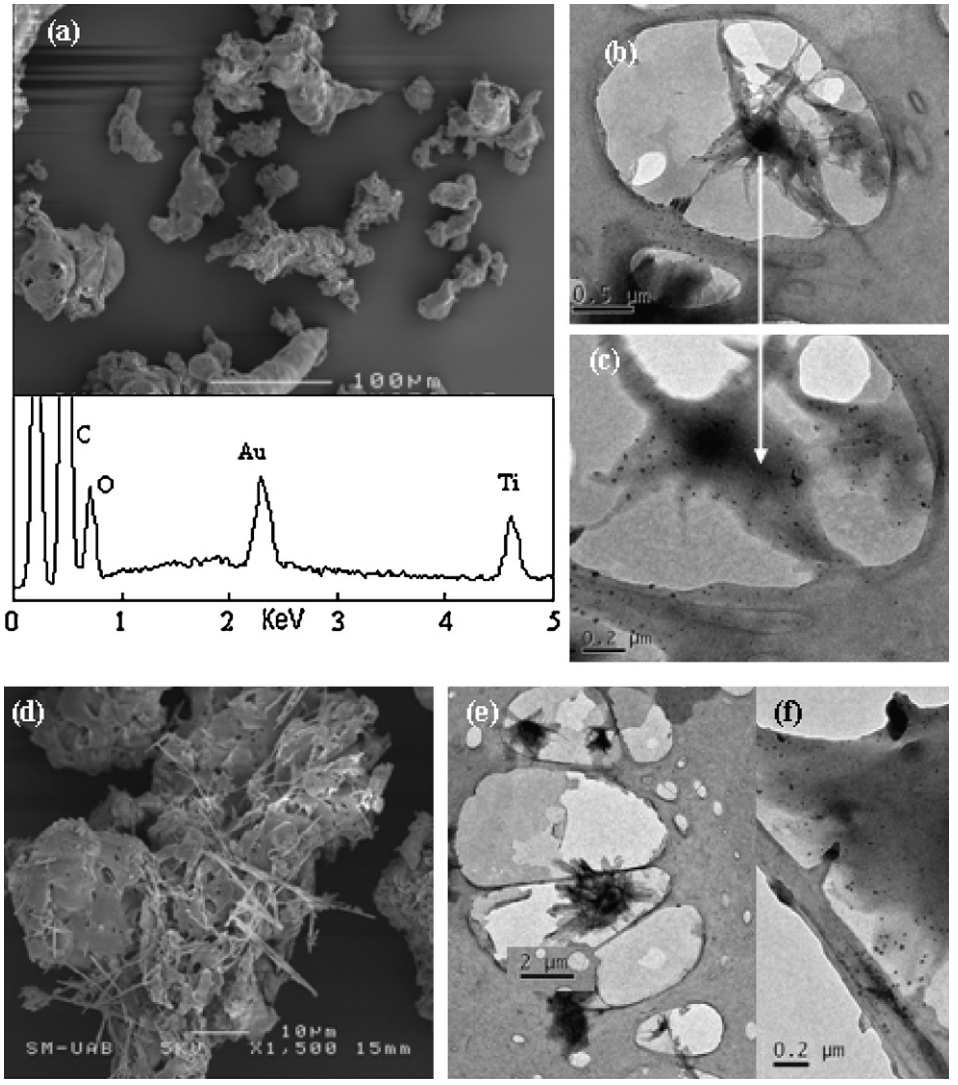

Fig. 8. Micrographs of PGSS® precipitated composite particles: (a) SEM with EDS analysis of sc-HCO:GMS:TiC_8 sample, (b) and (c) TEM of sc-HCO:GMS:TiC_8 sample, (d) SEM of sc-HCO:GMS:TiC_8:Caff sample, and (e) and (f) TEM of sc-HCO:GMS:TiC_8:Caff sample.

and 655 K for sc-HCO:GMS:TiC_{18} and sc-HCO:GMS:TiC_8, respectively, in Fig. 6b). An exact match at 670 K in the maximum rate of thermal decomposition was found for particles of sc-HCO:GMS and sc-HCO:GMS:TiC_{18} samples, indicating excellent interaction between the C_{18} alkyl chain of the silane monolayer on the TiO_2 surface and the tail groups of the lipids (also sterified with C_{18} carboxylic acids). The most thermally unstable composite was that constituted by lipids filled with bare TiO_2, which suggested a low affinity between the lipids and the hydrophilic surface of TiO_2 (Albertini et al., 2004).

According to XRD results, no noticeable influence of either bare or silanized TiO_2 nanoparticles on the crystallinity of solid lipids was observed (Fig. 7a). The presence of TiO_2 in the solid lipid particles was confirmed by the anatase peak at 25.3°. DSC analysis of the TiO_2 loaded samples showed the presence of two broad endothermic transitions with onsets at ~325 and 345 K, already observed for the PGSS® precipitated blend (Fig. 7b).

The macrostructure observed in the SEM pictures of the precipitated sc-HCO:GMS:TiC_8 sample (Fig. 8a) was similar to that found in the sc-HCO:GMS blend (Fig. 5a). The presence of TiO_2 within the lipidic matrix was confirmed by EDS measurements (Ti signal appeared at 4.6 keV in Fig. 8a). The microanalytical characterization was carried out in different areas of the precipitated blend. Results indicated that TiO_2 was dispersed with a relative high degree of homogeneity throughout the sample, and no segregated spots were observed. TiO_2 distribution was also studied by TEM imaging. Silanized TiO_2 particles were evenly distributed within the lipidic matrix, which can be clearly observed in the pores of some particles (Fig. 8b and c).

UV–vis spectra of samples containing C_8 silanized TiO_2 (sc-HCO:GMS:TiC_8) were recorded (Fig. 9) to study the UV-shielding ability of TiO_2 after dispersion in the solid lipid particles. Results indicated that TiO_2 and TiC_8 nanoparticles exhibited excellent UV-B (λ = 280–320 nm) and partial UV-A (λ = 320–400 nm) protection ability. Besides, the nanoparticles showed high transparency in the visible region due to the marked whiteness of the powder. Similar UV-protection ability was obtained for the silanized TiO_2 loaded lipid.

3.3. Incorporation of caffeine and release profile

For lipids that form highly crystalline particles the incorporation of drugs is difficult to achieve (Westesen et al., 1997; Müller et al., 2000). The decrease of crystallinity detected for the lipids in the mixture sc-HCO:GMS:TiC_8 with respect to raw lipidic materials was expected to facilitate the accommodation of active compounds in the matrix. Hence, preliminary experiments with the mixture of chemicals HCO:GMS:TiC_8:Caff (mass ratio of 1:1:0.1:0.2, which corresponded to a content of ~8 wt% in caffeine) processed by PGSS® were performed in order to examine the ability of caffeine incorporation to hybrid HCO:GMS:TiC_8 solid lipid particles. HPLC analysis of the resulting sc-HCO:GMS:TiC_8:Caff sample indicated that the caffeine content was ~4 wt%, which corresponded to 50 wt% of the initially added amount of caffeine to the mixing vessel. The caffeine loss was related with the relatively high solubility of this solute in $scCO_2$ under working conditions (Saldaña et al., 1999) and further precipitation inside the mixing vessel during decompression (Sampaio de Sousa et al., 2007).

SEM and TEM images of the sc-HCO:GMS:TiC_8:Caff sample showed the presence of needle-like caffeine crystals deposited on the solid lipid particles surface (Fig. 8d and e). TiO_2 nanoparticles could be also observed in some fractured crystals (Fig. 8f). The presence of caffeine crystals in the lipidic matrix was also noticed by means of XRD analysis, in which the peak appearing at $2\theta = 12°$ was attributed to the major peak of caffeine crystals (Fig. 7a). Hence, there was a limited inclusion of caffeine into the lipid particles. Complementary DSC studies showed that the melting peak of caffeine, occurring at ~510 K in the raw product, was not observed for the sc-HCO:GMS:TiC_8:Caff sample. This finding was due to the dissolution of caffeine crystals in the melted lipids during DSC analysis (Fig. 7b), as previously reported for other drugs (Sheu et al., 1994; Van den Mooter et al., 1998; Sethia and Squillante, 2002).

In an initial kinetic study, the release of the active compound into distilled water was investigated during 24 h, considered a regular time for topical sunscreen applications. The sc-HCO:GMS:TiC_8:Caff sample presented a two-step dissolution profile as shown in Fig. 10. The rapid dissolution burst of *ca.* 60 wt% of the caffeine content observed during the first few hours was

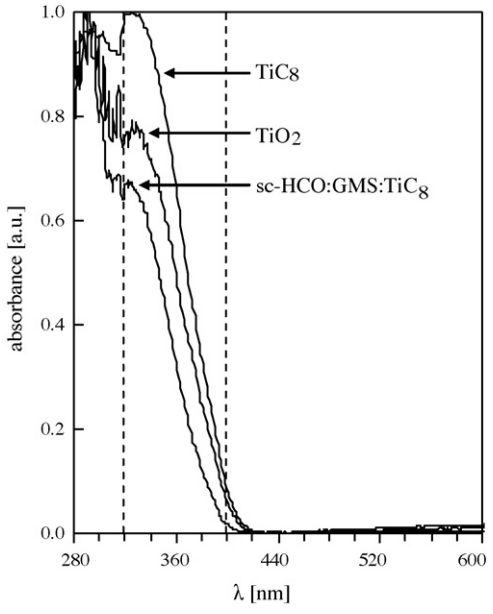

Fig. 9. UV–vis spectra of bare and silanized TiO_2 nanoparticles and TiC_8-loaded lipid particles. Vertical dashed lines indicate UV-B to UV-A (left) and UV-A to vis (right) transition regions.

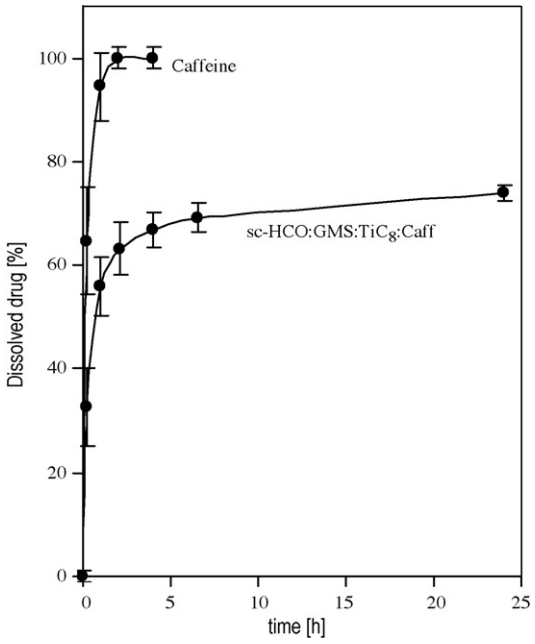

Fig. 10. Dissolution profiles in water of caffeine and precipitated lipid particles loaded with 4 wt% caffeine.

followed by a gradual dissolution of the remaining active agent. The dissolution profile of pristine caffeine particles in water, which occurs in 2 h (Fig. 10), is also given for comparison. The shape of the release profile of sc-HCO:GMS:TiC_8:Caff sample during the first 1 or 2 h was explained by the fast dissolution of the needle-like crystals of caffeine deposited on the solid lipid particles surface occurring first, followed by a prolonged dissolution of the caffeine entrapped within the lipids core.

4. Conclusions

Lipidic mixtures of HCO and GMS (50 wt%) were used to obtain composite powders of lipids, active agents (caffeine) and/or mineral fillers (silanized TiO_2) in presence of $scCO_2$. The mixed lipidic matrix crystallized into the β stable modification, but the decrease of the intensity of the reflection peaks indicated the formation of a relatively low ordered matrix. The reduction in crystallinity of the solid mixture of lipids can be strongly correlated with the ability of incorporating inorganic nanoparticles and drugs in the matrix. The matrix could be loaded with ~6 wt% silanized TiO_2 and ~4 wt% caffeine. Initial analysis indicated that caffeine-loaded solid lipid particles presented a two-step (fast and slow) dissolution profile, with an initial burst of 60 wt% of the loaded active agent. Lipid blends loaded with TiO_2 and caffeine have a potential application in sunscreens, since they encompassed the UV-filter behavior of TiO_2 and the photoaging prevention properties of caffeine. However, it should be stated that the caffeine release from similar particles incorporated in a sunscreen could be considerable different from that of the isolated particles analyzed here, which will be the study of a future work. The obtained lipid matrix has null toxicity for cosmetics and pharmaceutical dermal applications as well as a certain skin hydration effect.

Acknowledgements

The financial support of the Spanish projects MAT-2007-63355-E and CTQ2008-05370/PPQ are greatly acknowledged. C.A. García-González gives acknowledgment to CSIC for its funding support through I3P program.

References

Albertini, B., Passerine, N., González-Rodríguez, M.L., Perissutti, B., Rodríquez, L., 2004. Effect of Aerosil® on the properties of lipid controlled release microparticles. J. Control. Release 100, 233–246.
Bertin, C., Zunino, H., Pittet, J.C., Beau, P., Pineau, P., Massonneau, M., Robert, C., Hopkins, J., 2001. A double-bind evaluation of the activity of an anti-cellulite product containing retinol, caffeine and ruscogenine by a combination of several non-invasive methods. Int. J. Cosmet. Sci. 52, 199–210.
Bunjes, H., Westesen, K., Koch, M.H.J., 1996. Crystallization tendency and polymorphic transitions in triglyceride nanoparticles. Int. J. Pharm. 129, 159–173.
Calderone, M., Rodier, E., Letorneau, J.-J., Fages, J., 2007. Solidification of Precirol® by the expansion of a supercritical fluid saturated melt: from the thermodynamic balance towards the crystallization aspect. J. Supercrit. Fluids 42, 189–199.
Chacín, A., Vázquez, J.M., Müller, E.A., 1999. Molecular simulation of the Joule–Thomson inversion curve of carbon dioxide. Fluid Phase Equilib. 165, 147–155.
Chapman, D., 1962. The polymorphism of grlycerides. Chem. Rev. 62, 433–456.
Chattopadhyay, P., Shekunov, B.Y., Yim, D., Cipolla, D., Boyd, B., Farr, S., 2007. Production of solid lipid nanoparticle suspensions using supercritical fluid extraction of emulsions (SFEE) for pulmonary delivery using the AERx system. Adv. Drug Deliv. Rev. 59, 444–453.
Chen, H., Chang, X., Du, D., Liu, W., Liu, J., Weng, T., Yang, Y., Xu, H., Yang, X., 2006. Podophyllotoxin-loaded solid lipid nanoparticles for epidermal targeting. J. Control. Release 110, 296–306.
Davis, S.S., 2004. Coming of age of lipid-based drug delivery systems. Adv. Drug Del. Rev. 56, 1241–1242.
Fukné-Kokot, K., König, A., Knez, Z., Skerget, M., 2000. Comparison of different methods for determination of S-L-G equilibrium curve of a solid component in the presence of a compressed gas. Fluid Phase Equilib. 173, 297–310.
García-González, C.A., Andanson, J.M., Kazarian, S.G., Domingo, C., Saurina, J., 2009a. Application of principal component analysis to the thermal characterization of silanized nanoparticles obtained at supercritical carbon dioxide conditions. Anal. Chim. Acta 635, 227–234.
García-González, C.A., Fraile, J., López-Periago, A., Domingo, C., 2009b. Preparation of silane-coated TiO_2 nanoparticles in supercritical CO_2. J. Colloid Interface Sci. 338, 491–499.
Garti, N., Sato, K., 1988. Crystallization and Polymorphism of Fats and Fatty Acids. Marcel Dekker, New York.
Gasco, M.R., 1997. Solid lipid nanoparticles from warm microemulsions. Pharm. Technol. Eur. 9, 52–58.
González, S., Fernández-Lorente, M., Gilaberte-Calzada, Y., 2008. The latest on skin photoprotection. Clin. Dermatol. 26, 614–626.
Gopala Krishna, A.G., 1993. Influence of viscosity on wax settling and refining loss in rice bran oil. J. Am. Oil Chem. Soc. 70, 895–898.
Grobe, A., Renn, O., Jaeger, A., 2008. A report for IRGC: Risk Governance of Nanotechnology Applications in Food and Cosmetics. International Risk Governance Council, Geneva.
Hammam, H., Sivik, B., 1993. Phase behavior of some pure lipids in supercritical carbon dioxide. J. Supercrit. Fluids 6, 223–227.
Hexsel, C.L., Bangert, S.D., Hebert, A.A., Lim, H.W., 2008. Current sunscreen issues: 2007 Food and Drug Administration sunscreen labelling recommendations and combination sunscreen/insect repellent products. J. Am. Acad. Dermatol. 59, 316–323.
Himawan, C., Starov, V.M., Stapley, A.G.F., 2006. Thermodynamic and kinetic aspects of fat crystallization. Adv. Colloid Interface Sci. 122, 3–33.
Iwai, H., Fukasawa, J., Suzuki, T., 1996. Formation of stable lamellar structures with pseudo-ceramide. J. Colloid Interface Sci. 183, 13–17.
Jannin, V., Musakhanian, J., Marchaud, D., 2008. Approaches for the development of solid and semi-solid lipid-based formulations. Adv. Drug Deliv. Rev. 60, 734–746.
Kazarian, S.G., 2000. Polymer processing with supercritical fluids. Polym. Sci. C 42, 78–101.
Klöpffer, W., 2007. Nanotechnology and Life Cycle Assessment: A Systems Approach to Nanotechnology and Environment. Woodrow Wilson International Center for Scholars, Washington.
Kodali, D.R., Redgrave, T.G., Small, D.M., Atkinson, D., 1985. Synthesis and polymorphism of a homologous series of 3-acylsn-glycerols. Biochemistry 24, 519–525.
Kumar, V.V., Chandrasekar, D., Ramakrishna, S., Kishan, V., Rao, Y.M., Diwan, P.V., 2007. Development and evaluation of nitrendipine loaded solid lipid nanoparticles: Influence of wax and glycerid lipids on plasma pharmacokinetics. Int. J. Pharm. 335, 167–175.
Lambent Technologies, 2009. LUMULSE™ GMS K. Glycerol Monostearate. Technical Data Sheet, Available online in www.petroferm.com.
Ljusberg-Wahren, H., Nielsen, F.S., Brogard, M., Troedsson, E., Müllertz, A., 2005. Enzymatic characterization of lipid-based drug delivery systems. Int. J. Pharm. 298, 328–332.
Lowe, N.J., Shaath, N.A., Pathak, M.A., 1997. Sunscreens: Development, Evaluation, and Regulatory Aspects, Cosmetic Science and Technology Series, vol. 15, 2nd ed. Marcel Dekker, New York.
Müller, R.H., Mäder, K., Gohla, W., 2000. Solid lipid nanoparticles (SLN) for controlled drug delivery—a review of the state of the art. Eur. J. Pharm. Biopharm. 50, 161–177.
Müller, R.H., Radke, M., Wissing, S.A., 2002. Solid lipid nanoparticles and nanostructure lipid carriers in cosmetic and dermatological preparations. Adv. Drug. Deliv. Rev. 54, S131–S155.
Münüklü, P., Wubbolts, F., De Loos, T.W., Jansens, P.J., 2006. The phase behavior of systems of supercritical CO_2 or propane with edible fats and a wax. J. Supercrit. Fluids 39, 1–5.
Neubert, R., Wartewig, S., Wegener, M., Wienhold, A., 1997. Structure of stratum corneum lipids characterized by FT-Raman spectroscopy and DSC. II. Mixtures of ceramides and saturated fatty acids. Chem. Phys. Lipids 89, 3–14.
Ogunniyi, D.S., 2006. Castor oil: a vital industrial raw material. Bioresour. Technol. 97, 1086–1091.
Ohta, N., Hatta, I., 2002. Interaction among molecules in mixtures of ceramide/stearic acid, ceramide/cholesterol and ceramide/stearic acid/cholesterol. Chem. Phys. Lipids 115, 93–105.
Paoletti, R., Kritchevsky, D., 1967. Phase Diagrams of Triglyceride Systems. Advances in Lipid Research, vol. 5. Academic Press, New York.
Pardeike, J., Hommoss, A., Müller, R.H., 2009. Lipid nanoparticles (SLN, NLC) in cosmetic and pharmaceutical dermal products. Int. J. Pharm. 366, 170–184.
Plueddemann, E.P., 1991. Silane Coupling Agents, 2nd ed. Plenum Press, New York.
Puglia, C., Blasi, P., Rizza, L., Schoubben, A., Bonina, F., Rossi, C., Ricci, M., 2008. Lipid nanoparticles for prolonged topical delivery: an in vitro and in vivo investigation. Int. J. Pharm. 357, 295–304.
Rodrigues, M., Peiriço, N., Matos, H., Gomes de Azevedo, E., Lobato, M.R., Almeida, A.J., 2004. Microcomposites theophylline/hydrogenated palm oil from a PGSS process for controlled drug delivery systems. J. Supercrit. Fluids 29, 175–184.
Saldaña, M.D.A., Mohamed, R.S., Baer, M.G., Mazzafera, P., 1999. Extraction of purine alkaloids from Maté (Ilex paraguariensis) using supercritical CO_2. J. Agric. Food Chem. 47, 3804–3808.
Sampaio de Sousa, A.R., Calderone, M., Rodier, E., Fages, J., Duarte, C.M.M., 2006. Solubility of carbon dioxide in three lipid-based biocarriers. J. Supercrit. Fluids 39, 13–19.
Sampaio de Sousa, A.R., Silva, R., Tay, F.H., Simplício, A.L., Kazarian, S.G., Duarte, C.M.M., 2009. Solubility enhancement of trans-chalcone using lipid carriers and supercritical CO_2 processing. J. Supercrit. Fluids 48, 120–125.

Sampaio de Sousa, A.R., Simplício, A.L., de Sousa, H.C., Duarte, C.M.M., 2007. Preparation of glyceryl monostearate-based particles by PGSS®—application to caffeine. J. Supercrit. Fluids 43, 120–125.
Savolainen, M., Khoo, C., Glad, H., Dahlqvist, C., Juppo, A.M., 2002. Evaluation of controlled-release polar lipid microparticles. Int. J. Pharm. 244, 151–161.
Sethia, S., Squillante, E., 2004. Solid dispersion of carbamazepine in PVP K30 by conventional solvent evaporation and supercritical methods. Int. J. Pharm. 272, 1–10.
Sethia, S., Squillante, E., 2002. Physicochemical characterization of solid dispersions of carbamazepine formulated by supercritical carbon dioxide and conventional solvent evaporation method. J. Pharm. Sci. 91, 1948–1957.
Sheu, M.-T., Yeh, C.-M., Sokoloski, T.D., 1994. Characterization and dissolution of fenofibrate solid dispersion systems. Int. J. Pharm. 103, 137–146.
Siekmann, B., Westesen, K., 1994. Thermoanalysis of the recrystallization process of melt-homogenized glyceride nanoparticles. Colloids Surf. B 3, 159–175.
Spilimbergo, S., Luca, G., Elvassore, N., Bertucco, A., 2006. Effect of high-pressure gases on phase behaviour of solid lipids. J. Supercrit. Fluids 38, 289–294.
Staniforth, V., Chiu, L.-T., Yang, N.-S., 2006. Caffeic acid suppresses UVB radiation-induced expression of interleukin-10 and activation of mitogen-activated protein kinases in mouse. Carcinogenesis 27, 1803–1811.
Temelli, F., 2009. Perspectives on supercritical fluid processing of fats and oils. J. Supercrit. Fluids 47, 583–590.
Timms, R.E., 1984. Phase behavior of fats and their mixtures. Prog. Lipid Res. 23, 1–38.
Vali, A., Asilian, A., Khalesi, E., Khoddami, L., Shahtalebi, M., Mohammady, M., 2005. Evaluation of the efficacy of topical caffeine in the treatment of Psoriasis Vulgaris. J. Dermatol. Treat. 16, 234–237.
Van den Mooter, G., Augustijns, P., Blaton, N., Kinget, R., 1998. Physico-chemical characterization of solid dispersions of temazepam with polyethylene glycol 6000 and PVP K30. Int. J. Pharm. 164, 67–80.
Villalobos-Hernández, J.R., Müller-Goymann, C.C., 2005. Novel nanoparticulate carrier system based on carnauba wax and decyl oleate for the dispersion of inorganic sunscreens in aqueous media. Eur. J. Pharm. Biopharm. 60, 113–122.
Weidner, E., Knez, Z., Novak, Z., 1995. Process for preparing particles or powders, Patent WO95/21688, 17 August.
Westesen, K., Bunjes, H., Koch, M.H.J., 1997. Physicochemical characterization of lipid nanoparticles and evaluation of their drug loading capacity and sustained release potential. J. Control. Release 48, 223–236.
Yener, G., Incegül, T., Yener, N., 2003. Importance of using solid lipid microspheres as carriers for UV filters on the example octyl methoxy cinnamate. Int. J. Pharm. 258, 203–207.